Targeted Proteomic Analysis Reveals Enrichment of Atypical Ubiquitin Chains in Contractile Tissues

Tiaan Heunis[1,2], Frederic Lamoliatte[1,2], José Luis Marín-Rubio[1], Abeer Dannora[1] and Matthias Trost[1]*

[1]Biosciences Institute, Newcastle University, Newcastle upon Tyne, NE2 4HH, UK.

[2]These authors contributed equally to this work

*Corresponding author:

Matthias Trost, Tel: +44 191 2087009, E-mail: matthias.trost@ncl.ac.uk

Keywords

Parallel reaction monitoring; Absolute quantification; Ubiquitin chain-linkage composition; Atypical ubiquitin chain types; Primary murine macrophages; Murine tissues.

Data are available via ProteomeXchange with identifier PXD017754.

Username: reviewer39102@ebi.ac.uk

Password: vJ56s8uk

Abstract

Ubiquitylation is an elaborate post-translational modification involved in all biological processes. Its pleotropic effect is driven by the ability to form complex polyubiquitin chain architectures that can influence biological functions. In this study, we optimised sample preparation and chromatographic separation of Ubiquitin peptides for Absolute Quantification by Parallel Reaction Monitoring (Ub-AQUA-PRM). Using this refined Ub-AQUA-PRM assay, we were able to quantify all ubiquitin chain types in 10-minute LC-MS/MS runs. We used this method to determine the ubiquitin chain-linkage composition in murine bone marrow-derived macrophages and different mouse tissues. We could show tissue-specific differences in ubiquitin levels in murine tissues, with polyubiquitin chain types contributing a small proportion to the total pool of ubiquitin. Interestingly, we observed enrichment of atypical (K29 and K33) ubiquitin chains in heart and muscle. Ubiquitin profiling using tandem ubiquitin binding entities, directed at K29/K33 ubiquitin chains, and mass spectrometry analysis identified several mitochondrial proteins associated with these atypical ubiquitin chain types. Our approach enabled high-throughput screening of ubiquitin chain-linkage composition in different murine tissues and highlighted a possible role for atypical ubiquitylation in contractile tissues, likely associated with mitochondrial function. Our results contribute to our understanding of *in vivo* ubiquitin chain-linkage composition in murine tissues.

Significance

Large knowledge gaps exist in our understanding of ubiquitin chain-linkage composition in mammalian tissues. Defining this *in vivo* ubiquitin chain-linkage landscape could reveal the functional importance of different ubiquitin chain types in tissues. In this study, we refined the previously described Ub-AQUA-PRM assay to enable quantification of all ubiquitin chain types in a high-throughput manner. Using this assay, we provided new data on the ubiquitin chain-linkage composition in primary murine macrophages and tissues, and revealed an enrichment of atypical ubiquitin chains in contractile tissues. Our approach should thus enable rapid, high-throughput screening of ubiquitin chain-linkage composition in different sample types, as demonstrated in murine primary cells and tissues.

1. Introduction

Ubiquitylation is a post-translational modification (PTM) that results from the addition of ubiquitin, a 76 amino acid protein, to defined residues on substrate proteins. Ubiquitylation plays a role in practically all eukaryotic biological processes. It is therefore not surprising that aberrant ubiquitylation is linked to several human diseases, including cancer, infectious, neurodegenerative and developmental diseases [1]. A dedicated set of enzymes carry out substrate ubiquitylation in an orchestrated manner, resulting in the covalent attachment of ubiquitin to, generally, the ε-amino group of a lysine residue [2]. Ubiquitylation is reversible and deconjugation is controlled by ubiquitin-specific cysteine and metallo-proteases, known as deubiquitylases [3]. Protein substrates can be modified by monoubiquitin or can be polyubiquitylated, which is formed by further ubiquitylation of any lysine (K6, K11, K27, K29, K33, K48, and K63) or the N-terminal methionine (M1) of ubiquitin. This allows formation of complex chain architectures (homotypic, heterotypic or branched chains), which can ultimately influence a substrates fate [2]. For example, K48 and K11 chains target proteins for proteasomal degradation, while K63 and M1 are often involved in non-degradative processes like cell signalling, autophagy, DNA repair and innate immunity [2,4–11]. However, the biological functions of atypical and mixed ubiquitin chains are only beginning to emerge [8,12]. Detailed understanding of endogenous ubiquitin chain-linkage architecture is thus vital to unravel ubiquitin signalling and to reveal the functional importance of the ubiquitin code [13].

Recent technological advances in mass spectrometry-based proteomics has propelled this technology to the forefront of PTM analyses, including protein ubiquitylation [14,15]. Trypsin digestion of ubiquitylated proteins generate a characteristic di-glycine(diGly)-modified lysine residue that can be used to identify endogenous ubiquitylation sites. Antibody-based enrichment strategies directed at this diGly remnant, in combination with mass spectrometry, has facilitated the identification of tens of thousands of unique ubiquitylation sites on proteins [16–19]. This has shown an unprecedented role for ubiquitylation in all major biological processes in eukaryotes. Ubiquitin chain-linkage composition and architecture have been analysed by biochemical methods [20–22]. However, these methods currently lack throughput, are not quantitative and antibodies are only available for select ubiquitin linkage types. Mass spectrometry-based proteomics have initially been used to quantify endogenous levels of ubiquitin chain types by selected reaction monitoring (Ub-AQUA-SRM) [23]. This approach has subsequently been adapted to quadrupole-Orbitrap instruments using parallel reaction monitoring (PRM) [24]. Ub-AQUA-PRM has been used to determine chain-linkage composition of purified substrates [25], whole-cell lysates [26], to quantify K48-K63 branched chains [27,28], to gain information on

higher order chain-linkage architecture of ubiquitylated substrates [29] and to quantify phosphorylated and acetylated ubiquitin [30,31]. Even though ubiquitylation sites on proteins have been reported for murine tissues [19], the exact composition and absolute concentration of different ubiquitin chain types present in these different tissues are not well defined.

In this study, we refined the previously described Ub-AQUA-PRM method for absolute quantification of ubiquitin chain types. We optimised peptide oxidation, ion-pairing agents and implemented rapid, microflow chromatographic separation for increased assay sensitivity and throughput. We validated our Ub-AQUA-PRM assay using BMDMs treated with the proteasome inhibitor MG132, and could show an increase in all major ubiquitin chain types. Next, we showed the versatility of our assay by rapidly screening the ubiquitin chain-linkage composition in different murine tissues. We could show tissue-specific differences in total ubiquitin levels in murine tissues with an enrichment of atypical chains (K29 and K33) in heart and muscle. Affinity purification of proteins associated with K29/K33 ubiquitin chains, using tandem ubiquitin binding entities, followed by mass spectrometry analysis identified several mitochondrial proteins. Our refined Ub-AQUA-PRM assay is ideal for high-throughput screening of ubiquitin chain types, and highlighted a possible role for atypical ubiquitylation in contractile tissues.

2. Material and methods

2.1 Preparation of AQUA peptides

Synthetic ubiquitin peptides were obtained from Cambridge Research Biochemicals (Cleveland, United Kingdom) (Supplementary Table S1). Methionine-containing peptides were synthetised under their reduced form, and were subsequently oxidised during sample preparation, as described below. Peptides were dissolved at a concentration of 1 nmol/µl in 50:50 acetonitrile:water (v:v) and peptide purity was monitored by LC-MS/MS. Peptides lacking net peptide content were injected together with their isotope counterpart and net peptide content was determined based on the ratio between the two isotopes. Two sets of master mixes were prepared, with the 10 light and 10 heavy peptides mixed, separately, in equimolar concentrations. The light and heavy peptide master mixes were diluted, separately, to 10 pmol/µl in HPLC-grade water (Thermo Fisher Scientific) and stored at -80°C.

2.2 Optimisation of methionine oxidation and ion-pairing agents for targeted proteomic analysis

Methionine oxidation was optimised to generate a stable methionine sulfone for targeted proteomic analysis. Heavy and light peptides were mixed in a 1:1 ratio and incubated with different concentrations of H_2O_2 at either room temperature (RT) or 60°C. The conversion of reduced methionine to sulfoxide and sulfone derivatives were monitored by LC-MS/MS. The effect of ion-pairing agents on peptide retention and intensity was assessed by using increasing concentrations of formic acid (FA) and trifluoracetic acid (TFA) in the sample and loading buffers, as indicated in the text.

2.3 Preparation of standard curves

The heavy master mix was diluted to 100 fmol/µl and the light master mix was serially diluted from 10 pmol/µl to 1 amol/µl using a dilution factor of √10. The standard curve was prepared on ice by combining reaction components in the following order: 20 µl of HPLC-grade water, 10 µl of heavy mix at 100 fmol/µl, 10 µl of light mix at varying concentrations, 50 µl of 10% FA, and 10 µl of 10% H_2O_2. A second standard curve was prepared by substituting 10 µl of HPLC-grade water with 10 µl of *Escherichia coli* tryptic digest at 1 µg/µl. The *E. coli* tryptic digest was generated as described below. Samples were incubated for 2h at 60°C for oxidation, before targeted proteomic analysis.

2.4 Bacterial cell culture for proteomic analysis

E. coli DH5-α was cultured overnight in Luria-Bertani (Thermo Fisher Scientific) broth at 37°C with shaking at 180 rpm. The next day, cells were harvested (4,000 xg, 15 min, 4°C), washed twice with ice-cold PBS pH 7.4 and stored at -80°C until further analysis. Cell pellets were lysed in 5% SDS in 50 mM triethylammonium bicarbonate (TEAB) pH 7.5, by sonication. Whole-cell lysates were subsequently centrifuged (10,000 xg, 5 min, RT) and the supernatants used for proteomic sample preparation.

2.5 Murine cell culture and tissue collection

Animal work was approved by the Newcastle University ethical committee and performed under UK Home Office project licence (PCI 23A338). Bone marrow-derived macrophages (BMDMs) were derived from femurs of 8 to 12 week-old C57BL/6 mice. Bone marrow was extracted and differentiated into macrophages using Iscove's Modified Dulbecco's Media (IMDM; Sigma-Aldrich) supplemented with 10% heat-inactivated foetal calf serum (Thermo Fisher Scientific), 1% L-glutamine (Lonza), 1% penicillin/streptomycin (Lonza) and 20% L929-conditioned media for 7 days at 37 °C in 5% CO_2 humidified atmosphere. After differentiation, BMDMs were stimulated with 10 µM MG132 (Sigma-Aldrich) for 6 hours or mock treated. After stimulation, BMDMs were washed twice with ice-cold PBS pH 7.4. Cells were subsequently lysed by sonication in 5% SDS in 50 mM TEAB pH 7.5, supplemented

with 100 mM N-ethylmaleimide (NEM, Sigma-Aldrich) to inhibit deubiquitylases. Whole-cell lysates were used for proteomic sample preparation.

Tissues (brain, heart, lung, kidney, muscle and spleen) were collected from 8 to 12-week-old C57BL/6J mice, washed once with ice-cold PBS pH 7.4, flash frozen in liquid nitrogen and stored at -80°C until further analysis. Tissues were ground to a powder in liquid nitrogen using a mortar and pestle, and lysed by sonication in lysis buffer (5% SDS in 50 mM TEAB pH 7.5) supplemented with 100 mM NEM. Tissue lysates were subsequently centrifuged (10,000 xg, 5 min, RT) and the supernatants used for methanol chloroform precipitation. Proteins pellets were resuspended in lysis buffer and used for proteomic sample preparation.

2.6 Proteomics sample preparation

Protein concentration for all samples was determined using the bicinchoninic acid assay (BCA) assay (Thermo Fisher Scientific). Fifty µg of total protein was used for proteomics sample preparation by suspension trapping (S-Trap) [32], with minor modifications to that recommended by the supplier (ProtiFi, Huntington NY, USA). Samples were reduced with 5 mM tris(2-carboxyethyl)phosphine (Pierce) for 15 min at 37°C, and subsequently alkylated with 10 mM NEM for 15 min at room temperature in the dark. Five µl of 12% phosphoric acid was added to each sample after reduction and alkylation, followed by the addition of 330 µl S-Trap binding buffer (90% methanol in 100 mM TEAB pH 7.1). Acidified samples were added, separately, to S-Trap mini-spin columns and centrifuged at 4,000 xg for 1 minute. Each S-Trap mini-spin column was washed with 400 µl S-Trap binding buffer and centrifuged at 4,000 xg for 1 minute. This process was repeated for five washes. Twenty-five µl of 50 mM TEAB pH 8.0 containing sequencing-grade trypsin (1:10 ratio of trypsin:protein) was added to each sample, followed by proteolysis for 2 hours at 47°C using a thermomixer (Eppendorf). Peptides were eluted with 50 mM TEAB pH 8.0 and centrifugation at 1,000 xg for 1 minute. Elution steps were repeated using 0.2% FA and 0.2% FA in 50% acetonitrile, respectively. The three eluates from each sample were combined and dried using a speed-vac before storage at -80°C. Peptides were subsequently reconstituted to 1 µg/µl using 5% FA in water and prepared for PRM, on ice, by combining reagents in the following order: 30 µl of HPLC-grade water, 10 µl peptide digest at 1 µg/µl, 10 µl of heavy master mix at 100 fmol/µl, 40 µl of 10% FA and 10 µl of 10% H_2O_2. Samples were incubated for 2h at 60°C for oxidation before targeted mass spectrometry analysis.

2.7 Targeted LC-MS/MS analysis - Parallel Reaction Monitoring (PRM)

Peptide samples were injected on a Dionex Ultimate 3000 RSLC (Thermo Fisher Scientific) connected to a Q-Exactive HF mass spectrometer (Thermo Fisher Scientific). Fifty fmol of

each ubiquitin peptide was injected during analysis, along with 500 ng of tryptic peptide mixture from either *E. coli* or *Mus musculus* as indicated in the text. In order to minimise dead volume and shorten the analysis to only 10 min, we used a direct injection LC setup. During the loading phase, samples are loaded using a 5 µl loop and full loop injection, with a 2.4 µl needle and an overfill ratio of 1.5. Samples are injected onto a 150 µm x 150 mm EASY-Spray LC column (Thermo Fisher Scientific) using the nano-pump and 100% buffer A (96.9% HPLC-grade water, 3% DMSO, 0.1% FA) at 1.5 µl/min. After 4 min (6 µl), the column oven valve was switched to bypass the loop and peptides were eluted by increased concentration of buffer B (80% HPLC-grade acetonitrile, 16.9% HPLC-grade water, 3% DMSO, 0.1% FA) using a multistep gradient (Supplementary Table S2). The source was heated to 320°C and 2.5 kV was applied between the column emitter and the MS. The Q-Exactive HF was operated in PRM mode using a resolution of 15,000, AGC target of 2×10^5 and maximum injection time of 25 ms. Peptides were selected for MS/MS data acquisition using pre-determined isolation windows and fragmented using collision energies described in Supplementary Table S1.

2.8 Targeted proteomic data analysis

All Ub-AQUA-PRM RAW mass spectrometry files were analysed using Skyline-daily (version 4.1.1.11871) [33]. Fragment ion intensities were extracted and light to heavy (L/H) ratios of peptide pairs were automatically determined in Skyline. All extracted ion chromatograms were manually inspected. Standard curves were generated from log transformed L/H ratios and peptide concentrations, to determine the lower limit of detection (LLOD) and lower limit of quantification (LLOQ) for each peptide. The R^2 was determined based on the LLOQ of each peptide. Only curves with a R^2 value > 0.99 were used for determining the absolute concentration of total ubiquitin and the different ubiquitin chain types. Group comparisons were performed using a Student's t-test, and multiple group comparisons were performed using an analysis of variance (ANOVA), followed by a Tukey's HSD test for determining significance for pairwise comparisons, in GraphPad Prism (version 8.0.1).

2.9 Western blots

Total protein from brain, heart, kidney, lung, muscle and spleen were extracted as described above. Ten-microgram protein from each sample were separated on 12% SDS-PAGE gels before being electrotransferred to Immobilon-P transfer membranes (Merck Millipore). Membranes were probed with monoclonal antibody for mono-and polyubiquitylated proteins (FK2)(BML-PW8810; Enzo Life Sciences), anti-α-Tubulin (T9026; Sigma-Aldrich) and anti-Histone H3 (D1H2) (4499; Cell Signaling) antibodies. Corresponding secondary antibodies used included anti-mouse IgM, HRP-conjugated (AP307P; Sigma-Aldrich) and anti-rabbit

IgG, HRP-conjugated (7074; Cell Signaling Technology) antibodies. Peroxidase activity was developed using the Amersham™ ECL™ Prime Western Blotting Detection Reagent (GE Healthcare) and imaged on an Amersham Imager 600 digital imaging system (GE Healthcare). To assess equal loading of protein, Ponceau staining (Sigma-Aldrich) of the PVDF membranes was performed.

2.10 Bacterial cell culture for TUBE expression and purification

E. coli Rosetta-Gami (DE3) strains expressing tandem ubiquitin binding entities (TUBEs) directed against K29/K33 ubiquitin chain types were a kind gift from Dr. Yogesh Kulathu (MRC Protein Phosphorylation & Ubiquitylation Unit, University of Dundee, United Kingdom). These TUBEs were generated by cloning the ubiquitin binding domains of the ubiquitin thioesterase TRABID in tandem (DU24488). An M26A mutant in the TRABID ubiquitin binding domain, which abolishes ubiquitin binding, served as negative control (DU24534). Clones are available from the MRC Protein Phosphorylation & Ubiquitylation Unit, University of Dundee, United Kingdom. *E. coli* strains containing either pGEX-GST-HALO-TRABID or pGEX-GST-HALO-TRABID (M26A), further referred to as TRABIDm, were cultured overnight in LB broth containing 100 µg/ml ampicillin and 50 µg/ml chloramphenicol at 37°C with shaking at 180 rpm. The cultures were subsequently transferred to fresh LB broth, containing 100 µg/ml ampicillin and 50 µg/ml chloramphenicol, at 37°C with shaking at 180 rpm until an OD_{600nm} of 0.6-0.8 was reached. TRABID and TRABIDm expression was induced by the addition of 1 mM isopropyl β-d-1-thiogalactopyranoside (IPTG) and the *E. coli* cultures were incubated for 18 hours at 16°C. The next day, cells were harvested (4,000 xg, 15 min, 4°C), washed twice with ice-cold PBS pH 7.4 and stored at -80°C until further analysis. *E. coli* pellets were thawed on ice and resuspended in glutathione S-transferase (GST) lysis buffer (50 mM Tris-HCl pH 8.0, 100 mM NaCl, 5 mM β-mercaptoethanol and 1 mg/ml lysozyme). Cells were lysed by sonication (Fisherbrand Model 120 Sonic Dismembrator, Fisher Scientific), followed by centrifugation (4,000 xg, 20 min, 4°C) to pellet cellular debris. Glutathione sepharose high performance affinity chromatography medium (GE Healthcare) was used for GST-tagged TUBE purification from *E. coli* lysates.

Glutathione sepharose beads (1.25 ml of slurry) were washed with GST lysis buffer and centrifuged at 200 xg for 1 minute before the supernatant was discarded. This process was repeated for five washes in total. *E. coli* lysates were subsequently incubated with the beads for 1 h at 4°C under constant agitation to couple GST-tagged TUBE proteins. After incubation, the beads were washed with GST wash buffer (50 mM Tris-HCl pH 8.0, 500 mM NaCl and 5 mM β-mercaptoethanol) as described above. The beads were additionally washed once with PreScission cleavage buffer (50 mM Tris-HCl pH 8.0, 200 mM NaCl, 5

mM citrate, 25% glycerol and 5 mM β-mercaptoethanol), before the GST-tagged TUBE proteins were eluted from the beads using on-bead digestion with PreScission Protease (GE Healthcare). The beads were resuspended in PreScission cleavage buffer containing PreScission Protease (160 units) and samples were incubated overnight at 4°C under constant agitation. The supernatants, containing TUBE proteins, were collected and glycerol was added to a final concentration of 25% prior to storage at -20°C.

2.11 TUBE pulldown and sample preparation for mass spectrometry

Purified TUBE proteins were linked to HaloLink resin (Promega) before performing TUBE pulldowns from murine muscle. HaloLink resin (800 µl of slurry) was washed with Halo binding buffer (50 mM Tris-HCl pH 7.5, 150 mM NaCl, 0.05% NP40 and 5 mM β-mercaptoethanol), centrifuged at 200 xg for 1 minute and the supernatant discarded. This process was repeated for five washes in total. HaloLink resin (200 µl) was incubated with 10 nmol Halo-tagged TUBE protein overnight at 4°C with constant agitation. The beads were subsequently washed three times with Halo binding buffer before using as bait for pulldowns.

Murine muscle was harvested as previously described and lysed in non-denaturing lysis buffer (50 mM Tris-HCl pH 7.5, 250 mM NaCl, 1% NP40, 10% glycerol, protease inhibitors, 5 mM β-mercaptoethanol and 100 mM NEM) by sonication. Lysates were clarified by centrifugation (4,000 xg, 20 min, 4°C) before being used for TUBE pulldowns. Protein concentration was determined using a Bradford protein assay (Thermo Scientific). Lysates (12 mg) were pre-cleared by incubating with uncoupled HaloLink beads in non-denaturing lysis buffer, without NEM, for 30 minutes at 4°C with constant agitation to reduce non-specific binders. Samples were centrifuged at 200 xg for 1 minute and the supernatant incubated once more with uncoupled HaloLink beads. Supernatants were subsequently split into two, and either incubated with TRABID-linked HaloLink beads or TARBIDm-linked HaloLink beads overnight at 4°C with constant agitation. The next day, the samples were centrifuged at 200 xg for 1 minute and the supernatant discarded. Beads were washed with non-denaturing lysis buffer, without NEM, centrifuged at 200 xg for 1 minute and the supernatant discarded. This process was repeated for three washes in total. Proteins were eluted from the beads using lysis buffer (5% SDS in 50 mM TEAB pH 7.5) supplemented with 100 mM NEM. Elutes were processed for proteomic analysis as previously described, omitting the oxidation step.

2.12 LC-MS/MS analysis of TUBE pulldowns

Peptide samples from TUBE pulldowns were injected on a Dionex Ultimate 3000 RSLC (Thermo Fisher Scientific) connected to a Q-Exactive HF mass spectrometer (Thermo Fisher Scientific). Peptides were dissolved in 40 µl of 5% FA, and 5 µl of each sample was injected

onto an Acclaim PepMap 100 C18 LC trap column (100 µm ID × 20 mm, 3 µm, 100 Å), followed by separation on an EASY-Spray nanoLC C18 column (75 ID µm × 500 mm, 2 µm, 100 Å) at a flow rate of 300 nl/min. Solvent A was 96.9% HPLC-grade water, 3% DMSO and 0.1% FA. Solvent B was 80% HPLC-grade acetonitrile, 16.9% HPLC-grade water, 3% DMSO and 0.1% FA. The gradient used for analysis was as follows: solvent B was maintained at 1% for 5 min, followed by an increase from 1 to 35% B in 120 min, 35-90% B in 0.5 min, maintained at 90% B for 4 min, followed by a decrease to 3% in 0.5 min and equilibration at 3% for 10 min. The Q-Exactive HF was operated in positive-ion data-dependent mode. Precursor ion scans were performed in the Orbitrap in the range of 350-1,500 m/z with a resolution of 120,000 at 200 m/z, an automatic gain control (AGC) target of 1×10^6 and an ion injection time of 50 ms. The Top20 precursors were selected for MS/MS analysis in the Orbitrap after high-energy collisional dissociation (HCD) fragmentation. An HCD collision energy of 25% was used, the AGC target was set to 2×10^5 and a 50 ms injection time was allowed for MS/MS analysis. Dynamic exclusion of ions was implemented using a 45 s exclusion duration. An electrospray voltage of 2.0 kV and capillary temperature of 275°C, with no sheath and auxiliary gas flow, was used.

2.13 Discovery proteomics data analysis

All discovery proteomics RAW mass spectra were analysed using MaxQuant (version 1.6.7.0) [34], and searched against a SwissProt *Mus musculus* database (containing 25273 database entries with isoforms) downloaded on 13 November 2019. Peak list generation was performed within MaxQuant and searches were performed using default parameters and the built-in Andromeda search engine [35]. The enzyme specificity was set to consider fully tryptic peptides, and two missed cleavages were allowed. Oxidation of methionine, N-terminal acetylation and diglycine remnant on lysine residues were allowed as variable modifications. N-ethylmaleimide on cysteine was set as fixed modification. A protein and peptide false discovery rate (FDR) of less than 1% was employed in MaxQuant. Proteins that contained similar peptides and that could not be differentiated on the basis of MS/MS analysis alone were grouped to satisfy the principles of parsimony. Data handling and analysis was performed in Perseus (version 1.6.2.3) [36]. Reverse hits, contaminants and proteins only identified by site were removed before downstream statistical and bioinformatics analysis. Intensity data were transformed (log 2) and filtered to contain at least three valid values in one group for comparisons. Missing values were imputed using random numbers drawn from a normal distribution that simulates signals from low abundance proteins within Perseus. A Students t-test was performed to identify statistically significant differences between TRABID and TRABIDm pulldowns. Gene Ontology

enrichments were performed using ClusterProfiler [37], and pathway enrichments were performed using ReactomePA [38].

2.14 Data availability

The mass spectrometry proteomics data have been deposited to the ProteomeXchange [39] Consortium via the PRIDE [40] partner repository with the dataset identifier PXD017754. Reviewers can access it through the Username: reviewer39102@ebi.ac.uk and the password vJ56s8uk.

3. Results

3.1 Optimisation and refinement of Ub-AQUA-PRM

In order to analyse ubiquitin chain-linkage composition by PRM, we obtained 10 synthetic peptides as their light (endogenous) and heavy (standard) counterparts, which corresponds to the eight different ubiquitin chain types (M1, K6, K11, K27, K29, K33, K48 and K63) and two non-modified peptides (TITLEVEPSDTIENVK and ESTLHLVLR) that can serve as proxy for total ubiquitin (polyubiquitin, monoubiquitin and unconjugated ubiquitin). In order to maximise assay sensitivity, we set out to collapse all methionine-containing peptides into a single oxidation state (the methionine sulfone derivative), to optimise normalised collision energies for peptide fragmentation, and to evaluate different ion-pairing agents in the loading buffer for improved peptide retention and to minimise ion suppression.

Current Ub-AQUA-PRM strategies analyse the methionine sulfoxide version of methionine-containing peptides, induced by using low concentrations of H_2O_2 at 4°C [41,42]. As methionine sulfoxide can be reduced, we fully oxidised methionines into a sulfone derivative. Peptides were already partially oxidised, and the reduced version was barely detectable (<0.1% of the total intensity) when analysed using standard conditions for sample preparation (Supplementary Figure S1a, b). Interestingly, a methionine sulfone was present in more than 1% of the K6 peptide during initial analysis (Supplementary Figure S1b). We, therefore, optimised peptide oxidation to generate a methionine sulfone using H_2O_2. No difference in methionine sulfone-containing peptide (M1 or K6) intensity was observed without H_2O_2 at room temperature or at 60°C for 2 hours (Supplementary Figure S1a, b). However, a methionine sulfone was generated when using 0.1% H_2O_2 at 60°C for 2 hours, but the sulfoxide version still contributed substantially to M1 and K6 peptide intensity. Both methionine-containing peptides (M1 and K6) were converted into a stable methionine sulfone by more than 99.9%, based on peptide intensity, when using 1% H_2O_2 for 2h at 60°C

(Supplementary Figure S1 a, b). The other peptides analysed were unaffected under the same conditions (Supplementary Figure S1c). We therefore used 1% H_2O_2 for 2h at 60°C for peptide oxidation in all further analyses.

Next, we determined the optimal normalised collision energy (NCE) required for fragmenting each peptide, by infusing and fragmenting peptides using NCEs ranging from 10 to 40%. We defined the optimal NCE as the collision energy for which the top five fragment ions (excluding the y_1) were the most intense. Normalised collision energies ranged from 20% for the M1, K11, K63 and the TITTITLEVEPSDTIENVK unmodified ubiquitin peptide to 28% for the ESTESTLHLVLR unmodified ubiquitin peptide. Detailed information on NCE used for each peptide is available in Supplementary Table S1. Additionally, we also tested the effect of two commonly used ion-pairing agents in reversed-phase chromatography for their effect on peptide retention and ion intensity, namely FA and TFA. We compared FA and TFA at concentrations ranging from 0.2 to 5.0% (v:v) in the loading buffer (Supplementary Figure S2). For all these injections, buffer A and B remained the same. The K29 peptide is the most hydrophilic of the ubiquitin peptides, but we did not observe a major difference in peak intensity or peak shape between 5.0% FA and 0.2% TFA for this peptide (Supplementary Figure 2a). However, we observed a marked decrease in intensity for other ubiquitin peptides when using TFA, even as low as 0.2% (Supplementary Figure S2a, b). We therefore used 5.0% FA in the loading buffer for all further analyses.

Finally, we determined the lower limit of detection (LLOD) and lower limit of quantification (LLOQ) of each peptide in a simple (ubiquitin peptides only) and complex (*E. coli* tryptic digest) matrix. We opted for an *E. coli* tryptic digested as spike-in matrix as no endogenous ubiquitin is present in this organism that would interfere with the assay. LLOD for peptides were as low as 0.5 amol on column. In the simple matrix we could achieve LLOQ ranging from 50 amol for the M1 and K29 peptides to 1.5 fmol for the K11, K63 and TITTITLEVEPSDTIENVK ubiquitin peptides. Similar results were obtained for ubiquitin peptides in the complex matrix (Figure 1), reaching LLOQ as low as 0.1 fmol/µg protein injected. These results indicate that our refined Ub-AQUA-PRM assay could accurately quantify low levels of endogenous ubiquitin chain types in complex matrixes.

3.2 Absolute quantification of ubiquitin chain types in primary murine bone marrow-derived macrophages

We next set out to quantify ubiquitin chain types in primary murine macrophages (BMDMs). Additionally, we validated our Ub-AQUA-PRM assay using MG132, a proteasome inhibitor that results in ubiquitin accumulation, especially K48 chains [28,43]. We observed differences in the absolute concentration of total ubiquitin in control and MG132-treated

BMDMs, depending on the peptide used as proxy for total ubiquitin (Supplementary Figure S3). This could be due to different digestion kinetics of each peptide, or most likely because K63 linkages are more abundant than K11 in murine BMDMs, which will reduce ion intensity of the ESTESTLHLVLR peptide (Figure 2). However, both showed similar trends for total ubiquitin in the BMDMs (Supplementary Figure S3). Based on these results, we used the TITLEVEPSDTIENVK peptide as proxy for total ubiquitin. An increase in the percentage of polyubiquitin chains was observed in BMDMs after treatment with MG132, as would be expected (Figure 2a, b). All linkage types could be detected in murine BMDMs with K48 (63.2%), K63 (24.2%) and K29 (8.0%) contributing 95.4% of the total ubiquitin chain-linkage composition of whole-cell lysates (Figure 2c). Similarly, K48 (71.8%), K63 (15.5%) and K29 (5.2%) contributed 92.5% of the total ubiquitin chain-linkage composition of BMDMs during MG132 treatment (Figure 2d). Next, we determined whether there was any difference in ubiquitin chain types during treatment with MG132 for 6 hours. We observed a statistically significant increase in the majority of ubiquitin chain types, including total ubiquitin, during MG132 treatment (Figure 2e, Supplementary Figure S3). However, K11 and K27 chain types were below the limit of quantification during our analysis. These results indicate that K48, K63 and K29 linkage types dominate the ubiquitin chain-linkage compositions in murine BMDM whole-cell lysates and that up to ~29.2% of total ubiquitin is in the polyubiquitylated form in resting BMDMs.

3.3 Ubiquitin chain-linkage composition in murine tissues.

Using the refined Ub-AQUA-PRM assay, we screened the ubiquitin chain-linkage composition of six different murine tissues (brain, heart, kidney, lung, muscle and spleen) from three different mice. We were able to detect ubiquitin in all samples, with the brain, kidney and spleen having the highest levels of total ubiquitin (Figure 3). A statistically significant difference in total ubiquitin was observed in the brain, which had higher levels of total ubiquitin than the heart, lung and muscle (Figure 3). Interestingly, only a small percentage of total ubiquitin seems to be polyubiquitylated in murine tissues, with the contribution of chain types to total ubiquitin being ~1% in most tissues (Figure 4a). The lung had ~1.4% of total ubiquitin in the polyubiquitylated form, whereas muscle had the highest with ~8.7%. In most tissues, K48 was the most dominant chain type (Figure 4b), similar to what we observed in BMDMs. However, we observed marked differences in ubiquitin chain-linkage composition in heart and muscle. Interestingly, K33 was the most dominant chain type in heart and muscle (Figure 4b), contributing ~66.3% and ~76.1% of the total ubiquitin chain-linkage composition, respectively. Furthermore, K29 was enriched in the brain, heart, muscle and spleen. In order to determine the percentage contribution of these atypical linkage types to the total pool of ubiquitin, we normalised these chain types to total ubiquitin

in each of these tissues. Both K33 and K29 contributed only a small proportion to the total pool of ubiquitin, with <8% for K33 and <0.4% for K29, respectively (Supplementary Figure S4). These results indicate that there are tissue-specific differences in total ubiquitin and ubiquitin chain types in murine tissues, with atypical linkages increased in heart and muscle. Furthermore, our data indicate that only a small proportion of total ubiquitin in murine tissues are in the polyubiquitin form. It is therefore possible that many proteins in murine tissues are either monoubiquitylated, or that the majority of ubiquitin is in its unconjugated, free form. To test this hypothesis, we performed immunoblots for total ubiquitin (conjugated and unconjugated) using the same tissues analysed by Ub-AQUA-PRM. We observed high levels of unconjugated ubiquitin in the majority of tissues (Supplementary Figure S5). However, we did observe conjugated ubiquitin in all tissues. More unconjugated ubiquitin was observed in brain, kidney, lung and spleen, whereas heart and muscle had the least amount of unconjugated ubiquitin. In our Ub-AQUA-PRM assay, we also observed low levels of total ubiquitin in the heart and muscle, which corresponds to the data obtained with the western blots. This data indicates that there are major tissue-specific differences in ubiquitylation and that only a small proportion of total ubiquitin in murine tissues are in the conjugated form.

3.4 TUBE pulldowns identify muscle proteins associated with atypical polyubiquitin chain types.

We next performed tandem ubiquitin binding entity (TUBE) pulldowns, recognising K29/K33 ubiquitin chain types, using proteins from mouse muscle. We opted for using mouse muscle as this tissue contained the highest proportion of ubiquitin in the polyubiquitin, and specifically K33 polyubiquitin, form. Mass spectrometry analysis identified 899 proteins (Supplementary Table S3), of which 12 proteins (≥2-fold and p-value < 0.01) were determined to be enriched in the TRABID pulldowns when compared to the negative control (TRABIDm) (Table 1). From these proteins, we identified polyubiquitin as well as several proteins with Gene Ontology (GO) cellular component annotations associated with mitochondria (mitochondrial 2-oxoglutarate dehydrogenase, mitochondrial thioredoxin reductase 2, prohibitin and an aconitate hydratase) as enriched in the TRABID pulldowns. Prompted by this, we further performed GO enrichments for cellular components on an extended set of 71 proteins with a ≥2-fold change and p-value < 0.05 in our dataset (Supplementary Table S4), and found an enrichment for the mitochondrial membrane (Supplementary Figure 6a). Pathway enrichment of the same set of 71 proteins identified the TCA cycle and electron transport chain as most enriched pathways (Supplementary Figure 6b).

4. Discussion

Ubiquitin signalling is driven by the interplay between ubiquitin conjugation (mono- and polyubiquitylation) and deconjugation, which is controlled by a dedicated set of enzymes [2]. Unravelling this interplay at the protein, cell and tissue level is of utmost importance to understand ubiquitin signalling in mammalian systems. Mass spectrometry-based proteomics has become an essential approach for characterising ubiquitin signalling, including determining the absolute concentrations of the eight different ubiquitin chain types (M1, K6, K11, K27, K29, K33, K48 and K63).

In this study, we have refined the previously described ubiquitin absolute quantification mass spectrometry approach (Ub-AQUA-PRM) to enable quantification of all eight different ubiquitin chain types as well as total ubiquitin in 10-minute LC-MS/MS runs. Methionine-containing peptides can be challenging to analyse by PRM-based methods, as they can occur in different oxidation states [42]. This can become problematic for quantification when the peptide signal is divided across multiple oxidation states or, importantly, when there are differences between the endogenous peptide and the spike-in standard. Current Ub-AQUA-PRM methods have induced methionine oxidation and analysed the methionine sulfoxide-containing derivative of the N-terminal ubiquitin peptides (M1 and K6) [41,42]. It has previously been reported that methionine sulfoxide-containing ubiquitin peptides are stable for 21.5h, before oxidation state shifts have been observed [42]. We, however, opted to generate the more stable sulfone version of methionine to prevent any further oxidation shifts during sample analysis. In support of this, we already observed a methionine sulfone present in the K6 peptide when we obtained it from the supplier. We were able to generate a stable methionine sulfone and, importantly, did not observe any differences in oxidation or stability of the other ubiquitin peptides under the same conditions. This indicates that our oxidation procedure does not introduce undesirable artefacts.

Ion-pairing agents, such as trifluoroacetic acid, heptafluorobutyric acid and formic acid, are commonly used in liquid chromatography to enhance peptide interaction and retention on stationary phases [44]. A balance must, however, be obtained between ion suppression and improved chromatographic performance when using ion-pairing agents during liquid chromatography in combination with electrospray ionisation. Given the fact that several of the ubiquitin peptides are very hydrophilic and not well retained on pre-columns, most notably the K29 peptide, we were prompted to investigate the effect of ion-pairing agents on ubiquitin peptide separation and intensity during LC-MS/MS analysis [41]. Surprisingly, we observed no difference in K29 peptide intensity and peak shape when using

5% FA or 0.2% TFA for direct injection onto an analytical column. Higher concentrations of TFA, however, had a negative influence on methionine-containing peptide intensity and peak shape. Importantly, we observed higher peptide ion intensities when using FA for most other peptides. There is a well-documented suppressive effect of TFA on electrospray ionisation, which can negatively affect assay sensitivity [45–47]. Our data therefore indicates that 5% FA is an ideal ion-pairing agent for ubiquitin peptide analysis by LC-MS/MS, as it balances ion suppression and improved chromatographic performance for these peptides.

Using our refined Ub-AQUA-RPRM assay, we were able to obtain an LLOD of <0.5 amol and LLOQ ranging from 50 amol to1.5 fmol for the ubiquitin peptides. This indicates that our assay is able to probe the ubiquitin landscape to the same depth of other published assays, but within a fraction of the analysis time. We were prompted to investigate the ubiquitin chain-linkage composition in primary murine macrophages (BMDMs), given the importance of ubiquitin in innate immunity [5–7,11]. We could show that all possible ubiquitin chain types are present in BMDMs and that the absolute concentration of these different chain types spanned two orders of magnitude. K48, K63 and K29 dominated the chain-linkage landscape in BMDMs, which is in agreement with previous reports in cell lines [29,48]. Blocking proteasomal activity by MG132 increased the absolute concentration of all major ubiquitin chain types and resulted in an increase in total ubiquitin, which is also in agreement with previous reports [25,29,49]. Furthermore, we detected differences in total ubiquitin in six murine tissues, including brain, heart, kidney, lung, muscle and spleen. Interestingly, the contribution of polyubiquitin to total ubiquitin in murine tissues was low, the most prominent being 8.7% of total ubiquitin in the polyubiquitin form in muscle. In all other tissues studied, polyubiquitin contributed less than 1.5% of the total ubiquitin pool. Therefore, it seems that the majority of ubiquitin *in vivo* is in either the unconjugated or the monoconjugated form. Using western blots, we could show tissue-specific differences in levels of ubiquitylated proteins and unconjugated ubiquitin. It has been hypothesised that the energy requirements for ubiquitin conjugation is high and that the chain-elongating ability of ubiquitylating enzymes might be limited *in vivo* [29], which could limit formation of complex chain architectures. Unexpectedly, atypical linkage types (K29 and K33) were enriched in murine muscle and heart, compared to other tissues. K29-linked polyubiquitylation has been implicated in regulating Wnt signalling [50], in response to proteasomal stress [51] and in LRRK2 aggregation [52]. Further, K33-linked polyubiquitylation has been implicated in regulating cell-surface-receptor-mediated signal transduction [53] and protein trafficking [54]. K33-linked polyubiquitylation of coronin 7 enables the ubiquitin-dependent interaction between coronin 7 and Eps15, which is required for F-actin assembly and post-Golgi trafficking [54]. These studies all indicate a non-degradative role for K29- and K33-linked

polyubiquitylation. A previous report revealed several common enriched biological processes, including carbohydrate metabolism, proteolysis, muscle contraction and chromatin assembly, for ubiquitylated proteins from murine muscle and heart tissues [19]. Carbohydrate metabolism, energy generation and locomotion are vital roles of contractile organs [55] and it is therefore tempting to speculate that K29- and K33-linked polyubiquitylation could play an important, non-degradative role in these processes. We identified several mitochondrial proteins as enriched in TRABID pulldowns from mouse muscle, highlighting a possible role for atypical ubiquitin linkage types in mitochondrial function and metabolism. However, this warrants further investigation. Furthermore, the most enriched protein (based on fold change) was sorting nexin-6, a member of the nexin family involved in protein sorting in the endolysosomal system. This, additionally, highlights a role for K29- and/or K33- linked polyubiquitylation in non-degradative functions. Further analysis of the ubiquitylome and ubiquitin chain-linkage landscape, in combination with recently described methods such as Ub-clipping [48] and Ubiquitin Chain Enrichment Middle-Down Mass Spectrometry (UbiChEM-MS) [56], could reveal detailed information on atypical ubiquitylation and higher-order chain-linkage architecture in different tissues and pathological states.

5. Conclusion

Using optimised peptide oxidation, ion-pairing agents and microflow chromatographic separation, we could improve the Ub-AQUA-PRM assay to enable rapid, high-throughput screening of ubiquitin chain-linkage composition in different sample types within 10 min LC-MS/MS runs. We could show the presence of all eight ubiquitin chain types in primary cells and different tissues from C57BL/6 mice and revealed tissue-specific differences in ubiquitin levels. Our data is the first to reveal an enrichment of atypical ubiquitin chains in contractile tissues, and indicate an important role for these atypical chains in muscle and heart. Our results contribute to our understanding of the *in vivo* and *ex vivo* ubiquitin chain-linkage composition in murine tissues, and can form the basis for further analysis of atypical ubiquitin chains in mammalian systems.

Acknowledgements

The authors would like to thank Dr Yogesh Kulathu (MRC PPU, Dundee) for the gift of TUBE plasmids. This work was funded by a Wellcome Trust Investigator Award (215542/Z/19/Z) and the generous start-up funding of Newcastle University to MT. FL was funded by a Marie

Skłodowska-Curie Fellowship from the Horizon 2020 programme of the EU (project number 795670).

Conflict of interest

The authors declare no conflict of interest.

Author contributions

TH, FL and MT designed the study. TH and FL performed all mass spectrometry experiments and data analysis. JLM-R performed western blots. AD was responsible for animal husbandry and animal experimental procedures. TH and MT wrote the paper with contribution of all authors.

References

[1] M. Rape, Post-translational modifications: Ubiquitylation at the crossroads of development and disease, Nat. Rev. Mol. Cell Biol. 19 (2018) 59–70. doi:10.1038/nrm.2017.83.

[2] K.N. Swatek, D. Komander, Ubiquitin modifications, Cell Res. 26 (2016) 399–422. doi:10.1038/cr.2016.39.

[3] D. Komander, M.J. Clague, S. Urbé, Breaking the chains: Structure and function of the deubiquitinases, Nat. Rev. Mol. Cell Biol. 10 (2009) 550–563. doi:10.1038/nrm2731.

[4] W. Chen, D. Li, H. Mei, R.A. Giridhar, I. Jun-ichiro, J.C. Zhijian, TAK1 is a ubiquitin-dependent kinase of MKK and IKK, Nature. 412 (2001) 1–11.

[5] L. Deng, C. Wang, E. Spencer, L. Yang, A. Braun, J. You, C. Slaughter, C. Pickart, Z.J. Chen, Activation of the Iκb kinase complex by TRAF6 requires a dimeric ubiquitin-conjugating enzyme complex and a unique polyubiquitin chain, Cell. 103 (2000) 351–361. doi:10.1016/S0092-8674(00)00126-4.

[6] F. Tokunaga, S.I. Sakata, Y. Saeki, Y. Satomi, T. Kirisako, K. Kamei, T. Nakagawa, M. Kato, S. Murata, S. Yamaoka, M. Yamamoto, S. Akira, T. Takao, K. Tanaka, K. Iwai, Involvement of linear polyubiquitylation of NEMO in NF-κB activation, Nat. Cell Biol. 11 (2009) 123–132. doi:10.1038/ncb1821.

[7] B. Gerlach, S.M. Cordier, A.C. Schmukle, C.H. Emmerich, E. Rieser, T.L. Haas, A.I. Webb, J.A. Rickard, H. Anderton, W.W.L. Wong, U. Nachbur, L. Gangoda, U. Warnken, A.W. Purcell, J. Silke, H. Walczak, Linear ubiquitination prevents inflammation and regulates immune signalling, Nature. 471 (2011) 591–596. doi:10.1038/nature09816.

[8] C.N. Cunningham, J.M. Baughman, L. Phu, J.S. Tea, C. Yu, M. Coons, D.S. Kirkpatrick, B. Bingol, J.E. Corn, USP30 and parkin homeostatically regulate atypical ubiquitin chains on mitochondria, Nat. Cell Biol. 17 (2015) 160–169. doi:10.1038/ncb3097.

[9] C. Hoege, B. Pfander, G.L. Moldovan, G. Pyrowolakis, S. Jentsch, RAD6-dependent DNA repair is linked to modification of PCNA by ubiquitin and SUMO, Nature. 419 (2002) 135–141. doi:10.1038/nature00991.

[10] C. Doil, N. Mailand, S. Bekker-Jensen, P. Menard, D.H. Larsen, R. Pepperkok, J. Ellenberg, S. Panier, D. Durocher, J. Bartek, J. Lukas, C. Lukas, RNF168 binds and amplifies ubiquitin conjugates on damaged chromosomes to allow accumulation of repair proteins, Cell. 136 (2009) 435–446. doi:10.1016/j.cell.2008.12.041.

[11] M.U. Gack, Y.C. Shin, C.H. Joo, T. Urano, C. Liang, L. Sun, O. Takeuchi, S. Akira, Z. Chen, S. Inoue, J.U. Jung, TRIM25 RING-finger E3 ubiquitin ligase is essential for RIG-I-mediated antiviral activity, Nature. 446 (2007) 916–920. doi:10.1038/nature05732.

[12] H.J. Meyer, M. Rape, Enhanced protein degradation by branched ubiquitin chains, Cell. 157 (2014) 910–921. doi:10.1016/j.cell.2014.03.037.

[13] D. Komander, M. Rape, The ubiquitin code, Annu. Rev. Biochem. 81 (2012) 203–229. doi:10.1146/annurev-biochem-060310-170328.

[14] R.E. Heap, M.S. Gant, F. Lamoliatte, J. Peltier, M. Trost, Mass spectrometry techniques for studying the ubiquitin system, Biochem. Soc. Trans. 45 (2017) 1137–1148. doi:10.1042/BST20170091.

[15] A. Ordureau, C. Münch, J.W. Harper, Quantifying ubiquitin signaling, Mol. Cell. 58 (2015) 660–676. doi:10.1016/j.molcel.2015.02.020.

[16] G. Xu, J.S. Paige, S.R. Jaffrey, Global analysis of lysine ubiquitination by ubiquitin remnant immunoaffinity profiling, Nat. Biotechnol. 28 (2010) 868–873. doi:10.1038/nbt.1654.

[17] N.D. Udeshi, P. Mertins, T. Svinkina, S.A. Carr, Large-scale identification of ubiquitination sites by mass spectrometry, Nat. Protoc. 8 (2013) 1950. https://doi.org/10.1038/nprot.2013.120.

[18] A.E.H. Elia, A.P. Boardman, D.C. Wang, E.L. Huttlin, R.A. Everley, N. Dephoure, C. Zhou, I. Koren, S.P. Gygi, S.J. Elledge, Quantitative proteomic atlas of ubiquitination and acetylation in the DNA damage response, Mol. Cell. 59 (2015) 867–881. doi:10.1016/j.molcel.2015.05.006.

[19] S.A. Wagner, P. Beli, B.T. Weinert, C. Schölz, C.D. Kelstrup, C. Young, M.L. Nielsen, J. V. Olsen, C. Brakebusch, C. Choudhary, Proteomic analyses reveal divergent ubiquitylation site patterns in murine tissues, Mol. Cell. Proteomics. 11 (2012) 1578–1585. doi:10.1074/mcp.M112.017905.

[20] M.K. Hospenthal, T.E.T. Mevissen, D. Komander, Deubiquitinase-based analysis of ubiquitin chain architecture using Ubiquitin Chain Restriction (UbiCRest), Nat. Protoc. 10 (2015) 349–361. doi:10.1038/nprot.2015.018.

[21] S.J. van Wijk, S. Fulda, I. Dikic, M. Heilemann, Visualizing ubiquitination in mammalian cells, EMBO Rep. 20 (2019) 1–18. doi:10.15252/embr.201846520.

[22] R.G. Yau, K. Doerner, E.R. Castellanos, D.L. Haakonsen, A. Werner, N. Wang, X.W. Yang, N. Martinez-Martin, M.L. Matsumoto, V.M. Dixit, M. Rape, Assembly and function of heterotypic ubiquitin chains in cell-cycle and protein qualitycontrol, Cell. (2017). doi:10.1016/j.cell.2017.09.040.

[23] D.S. Kirkpatrick, N.A. Hathaway, J. Hanna, S. Elsasser, J. Rush, D. Finley, R.W. King, S.P. Gygi, Quantitative analysis of in vitro ubiquitinated cyclin B1 reveals complex chain topology, Nat. Cell Biol. 8 (2006) 700–710. doi:10.1038/ncb1436.

[24] H. Tsuchiya, K. Tanaka, Y. Saeki, The parallel reaction monitoring method contributes to a highly sensitive polyubiquitin chain quantification, Biochem. Biophys. Res. Commun. (2013). doi:10.1016/j.bbrc.2013.05.080.

[25] H. Tsuchiya, F. Ohtake, N. Arai, A. Kaiho, S. Yasuda, K. Tanaka, Y. Saeki, In vivo ubiquitin linkage-type analysis reveals that the Cdc48-Rad23/Dsk2 axis contributes to K48-linked chain specificity of the proteasome, Mol. Cell. (2017). doi:10.1016/j.molcel.2017.04.024.

[26] T.P. Miettinen, J. Peltier, A. Härtlova, M. Gierliński, V.M. Jansen, M. Trost, M. Björklund, Thermal proteome profiling of breast cancer cells reveals proteasomal activation by CDK 4/6 inhibitor palbociclib, EMBO J. 37 (2018) 1–19.

doi:10.15252/embj.201798359.

[27] F. Ohtake, Y. Saeki, S. Ishido, J. Kanno, K. Tanaka, The K48-K63 branched ubiquitin chain regulates NF-κB signaling, Mol. Cell. 64 (2016) 251–266. doi:10.1016/j.molcel.2016.09.014.

[28] F. Ohtake, H. Tsuchiya, Y. Saeki, K. Tanaka, K63 ubiquitylation triggers proteasomal degradation by seeding branched ubiquitin chains, Proc. Natl. Acad. Sci. U. S. A. 115 (2018) E1401–E1408. doi:10.1073/pnas.1716673115.

[29] H. Tsuchiya, D. Burana, F. Ohtake, N. Arai, A. Kaiho, M. Komada, K. Tanaka, Y. Saeki, Ub-ProT reveals global length and composition of protein ubiquitylation in cells, Nat. Commun. 9 (2018). doi:10.1038/s41467-018-02869-x.

[30] F. Koyano, K. Okatsu, H. Kosako, Y. Tamura, E. Go, M. Kimura, Y. Kimura, H. Tsuchiya, H. Yoshihara, T. Hirokawa, T. Endo, E.A. Fon, J.F. Trempe, Y. Saeki, K. Tanaka, N. Matsuda, Ubiquitin is phosphorylated by PINK1 to activate parkin, Nature. 510 (2014) 162–166. doi:10.1038/nature13392.

[31] F. Ohtake, Y. Saeki, K. Sakamoto, K. Ohtake, H. Nishikawa, H. Tsuchiya, T. Ohta, K. Tanaka, J. Kanno, Ubiquitin acetylation inhibits polyubiquitin chain elongation, EMBO Rep. 16 (2015) 192–201. doi:10.15252/embr.201439152.

[32] M. HaileMariam, R.V. Eguez, H. Singh, S. Bekele, G. Ameni, R. Pieper, Y. Yu, S-Trap, an ultrafast sample-preparation approach for shotgun proteomics, J. Proteome Res. 17 (2018) 2917–2924. doi:10.1021/acs.jproteome.8b00505.

[33] B. MacLean, D.M. Tomazela, N. Shulman, M. Chambers, G.L. Finney, B. Frewen, R. Kern, D.L. Tabb, D.C. Liebler, M.J. MacCoss, Skyline: An open source document editor for creating and analyzing targeted proteomics experiments, Bioinformatics. 26 (2010) 966–968. doi:10.1093/bioinformatics/btq054.

[34] J. Cox, M. Mann, MaxQuant enables high peptide identification rates, individualized p.p.b.-range mass accuracies and proteome-wide protein quantification, Nat. Biotechnol. 26 (2008) 1367–1372. doi:10.1038/nbt.1511.

[35] J. Cox, N. Neuhauser, A. Michalski, R.A. Scheltema, J. V. Olsen, M. Mann, Andromeda: A peptide search engine integrated into the MaxQuant environment, J. Proteome Res. 10 (2011) 1794–1805. doi:10.1021/pr101065j.

[36] S. Tyanova, T. Temu, P. Sinitcyn, A. Carlson, M.Y. Hein, T. Geiger, M. Mann, J. Cox, The Perseus computational platform for comprehensive analysis of (prote)omics data,

Nat. Methods. 13 (2016) 731–740. doi:10.1038/nmeth.3901.

[37] G. Yu, L.G. Wang, Y. Han, Q.Y. He, ClusterProfiler: An R package for comparing biological themes among gene clusters, Omi. A J. Integr. Biol. 16 (2012) 284–287. doi:10.1089/omi.2011.0118.

[38] G. Yu, Q.Y. He, ReactomePA: An R/Bioconductor package for reactome pathway analysis and visualization, Mol. Biosyst. 12 (2016) 477–479. doi:10.1039/c5mb00663e.

[39] E.W. Deutsch, A. Csordas, Z. Sun, A. Jarnuczak, Y. Perez-Riverol, T. Ternent, D.S. Campbell, M. Bernal-Llinares, S. Okuda, S. Kawano, R.L. Moritz, J.J. Carver, M. Wang, Y. Ishihama, N. Bandeira, H. Hermjakob, J.A. Vizcaíno, The ProteomeXchange consortium in 2017: Supporting the cultural change in proteomics public data deposition, Nucleic Acids Res. 45 (2017) D1100–D1106. doi:10.1093/nar/gkw936.

[40] Y. Perez-Riverol, A. Csordas, J. Bai, M. Bernal-Llinares, S. Hewapathirana, D.J. Kundu, A. Inuganti, J. Griss, G. Mayer, M. Eisenacher, E. Pérez, J. Uszkoreit, J. Pfeuffer, T. Sachsenberg, Ş. Yilmaz, S. Tiwary, J. Cox, E. Audain, M. Walzer, A.F. Jarnuczak, T. Ternent, A. Brazma, J.A. Vizcaíno, The PRIDE database and related tools and resources in 2019: Improving support for quantification data, Nucleic Acids Res. 47 (2019) D442–D450. doi:10.1093/nar/gky1106.

[41] H. Tsuchiya, K. Tanaka, Y. Saeki, The parallel reaction monitoring method contributes to a highly sensitive polyubiquitin chain quantification, Biochem. Biophys. Res. Commun. 436 (2013) 223–229. doi:10.1016/j.bbrc.2013.05.080.

[42] L. Phu, A. Izrael-Tomasevic, M.L. Matsumoto, D. Bustos, J.N. Dynek, A. V. Fedorova, C.E. Bakalarski, D. Arnott, K. Deshayes, V.M. Dixit, R.F. Kelley, D. Vucic, D.S. Kirkpatrick, Improved quantitative mass spectrometry methods for characterizing complex ubiquitin signals, Mol. Cell. Proteomics. 10 (2011) 1–19. doi:10.1074/mcp.M110.003756.

[43] K.L. Rock, C. Gramm, L. Rothstein, K. Clark, R. Stein, L. Dick, D. Hwang, A.L. Goldberg, Inhibitors of the proteasome block the degradation of most cell proteins and the generation of peptides presented on MHC class I molecules, Cell. (1994). doi:10.1016/S0092-8674(94)90462-6.

[44] M.T.W. Hancock, W.S., Bishop, C.A., Prestidge, R.L., Harding, D.R.K., Hearn, Reversed-phase, high-pressure liquid chromatography of, Science (80-.). 200 (1978)

1168–1171.

[45] T.M. Annesley, Ion suppression in mass spectrometry, Clin. Chem. 49 (2003) 1041–1044. doi:10.1373/49.7.1041.

[46] J. Eshraghi, S.K. Chowdhury, Factors affecting electrospray ionization of effluents containing trifluoroacetic acid for high-performance liquid chromatography/mass spectrometry, Anal. Chem. 65 (1993) 3528–3533. doi:10.1021/ac00071a035.

[47] M. Nshanian, R. Lakshmanan, H. Chen, R.R.O. Loo, J.A. Loo, Enhancing sensitivity of liquid chromatography–mass spectrometry of peptides and proteins using supercharging agents, Int. J. Mass Spectrom. (2018). doi:10.1016/j.ijms.2017.12.006.

[48] K.N. Swatek, J.L. Usher, A.F. Kueck, C. Gladkova, T.E.T. Mevissen, J.N. Pruneda, T. Skern, D. Komander, Insights into ubiquitin chain architecture using Ub-clipping, Nature. (2019). doi:10.1038/s41586-019-1482-y.

[49] F. Ohtake, H. Tsuchiya, Y. Saeki, K. Tanaka, K63 ubiquitylation triggers proteasomal degradation by seeding branched ubiquitin chains, Proc. Natl. Acad. Sci. 115 (2018) E1401–E1408. doi:10.1073/PNAS.1716673115.

[50] C. Fei, Z. Li, C. Li, Y. Chen, Z. Chen, X. He, L. Mao, X. Wang, R. Zeng, L. Li, Smurf1-mediated Lys29-linked nonproteolytic polyubiquitination of axin negatively regulates Wnt/catenin signaling, Mol. Cell. Biol. 33 (2013) 4095–4105. doi:10.1128/mcb.00418-13.

[51] H.C. Besche, Z. Sha, N. V. Kukushkin, A. Peth, E.M. Hock, W. Kim, S. Gygi, J.A. Gutierrez, H. Liao, L. Dick, A.L. Goldberg, Autoubiquitination of the 26S proteasome on Rpn13 regulates breakdown of ubiquitin conjugates, EMBO J. 33 (2014) 1159–1176. doi:10.1002/embj.201386906.

[52] F.C. Nucifora, L.G. Nucifora, C.H. Ng, N. Arbez, Y. Guo, E. Roby, V. Shani, S. Engelender, D. Wei, X.F. Wang, T. Li, D.J. Moore, O. Pletnikova, J.C. Troncoso, A. Sawa, T.M. Dawson, W. Smith, K.L. Lim, C.A. Ross, Ubiqutination via K27 and K29 chains signals aggregation and neuronal protection of LRRK2 by WSB1, Nat. Commun. 7 (2016) 1–11. doi:10.1038/ncomms11792.

[53] H. Huang, M. shin Jeon, L. Liao, C. Yang, C. Elly, J.R. Yates, Y.C. Liu, K33-linked polyubiquitination of T cell receptor-ζ regulates proteolysis-independent T cell signaling, Immunity. 33 (2010) 60–70. doi:10.1016/j.immuni.2010.07.002.

[54] W.C. Yuan, Y.R. Lee, S.Y. Lin, L.Y. Chang, Y.P. Tan, C.C. Hung, J.C. Kuo, C.H. Liu,

M.Y. Lin, M. Xu, Z.J. Chen, R.H. Chen, K33-linked polyubiquitination of coronin 7 by Cul3-KLHL20 ubiquitin E3 ligase regulates protein trafficking, Mol. Cell. 54 (2014) 586–600. doi:10.1016/j.molcel.2014.03.035.

[55] A.S. Deshmukh, M. Murgia, N. Nagaraj, J.T. Treebak, J. Cox, M. Mann, Deep proteomics of mouse skeletal muscle enables quantitation of protein isoforms, metabolic pathways, and transcription factors, Mol. Cell. Proteomics. 14 (2015) 841–853. doi:10.1074/mcp.M114.044222.

[56] S.O. Crowe, A.S.J.B. Rana, K.K. Deol, Y. Ge, E.R. Strieter, Ubiquitin chain enrichment middle-down mass spectrometry enables characterization of branched ubiquitin chains in cellulo, Anal. Chem. 89 (2017) 4428–4434. doi:10.1021/acs.analchem.6b03675.

Figure legends

Figure 1. Limits of detection and quantification of spiked-in, heavy and light ubiquitin peptides in an *E. coli* proteome digest. Standard curves were generated using 10 synthetic ubiquitin peptides in their light and heavy counterparts. Heavy peptides were used at 10 fmol/µl, while light peptides were serially diluted from 1 pmol/µl to 1 amol/µl. Peptides were oxidised using H_2O_2 before injected on a Q-Exactive HF mass spectrometer for PRM analysis. The peptide master mix contained each of the eight different ubiquitin chain-type peptides (a-h) and two peptides that served as proxy for total ubiquitin (i, j). Error bars indicate standard deviation.

Figure 2. All eight polyubiquitin chain types are present in murine bone marrow-derived macrophages. Percentage of polyubiquitin chain types present in resting, unstimulated (a) and MG132-treated (b) bone marrow-derived macrophages, compared to the total pool of ubiquitin. Contribution of each of the eight different ubiquitin chain types to the total pool of polyubiquitin in resting, unstimulated (c) and MG132-treated bone marrow-derived macrophages (d). MG132 treatment caused a statistically significant increase in all quantified ubiquitin chain types (e), as well as total ubiquitin (Supplementary Figure S3). Statistical significance is denoted with an * and indicates a p-value < 0.05 determined using a Student's t-test. Error bars indicate standard deviation.

Figure 3. Murine tissues contain different levels of ubiquitin. Absolute concentration of ubiquitin in different murine tissues when using non-modified peptides as proxy for total ubiquitin. Total ubiquitin was derived from the sum of the absolute concentrations of TITLEVPSDTIENVK and K11 ubiquitin peptides. Statistical significance is denoted with an *

and indicates an adjusted p-value < 0.05 after a Tukey's HSD test and ANOVA. Error bars indicate standard deviation.

Figure 4. Tissue-specific differences in ubiquitin chain types and compositions exist in murine tissues. (a) Percentage of polyubiquitin chain types present in different murine tissues, compared to the total pool of ubiquitin present in these tissues. (b) Contribution of each of the eight different ubiquitin chain types to the total pool of polyubiquitin in different murine tissues. Error bars indicate standard deviation.

Table 1. Proteins enriched in TRABID pulldowns from mouse muscle.

Supporting documents

Supplementary Figure S1. Generation of a stable methionine sulfone by oxidation. Methionine-containing ubiquitin peptides were oxidised using hydrogen peroxide and analysed by LC-MS/MS to determine the generation of a methionine sulfone. A stable methionine sulfone was generated using 1.0% H_2O_2 at 60°C for 2 hours in M1 (a) and K6 (b) peptides. (c) Peptide intensities observed for non-methionine-containing ubiquitin peptides when using hydrogen peroxide for oxidation. L = light version of the peptide, H = heavy version of the peptide, LoD = limit of detection. Error bars indicate standard deviation.

Supplementary Figure S2. Formic acid is a superior ion-pairing agent for ubiquitin peptides. (a) Peptide intensities observed for M1, K6 and K29 ubiquitin peptides when using formic acid (FA) and trifluoroacetic acid (TFA) as ion-pairing agent in the loading buffer. (b) Peptide intensities observed for the other ubiquitin peptides when using FA and TFA in the loading buffer. L = light version of the peptide, H = heavy version of the peptide, LoD = limit of detection. Error bars indicate standard deviation.

Supplementary Figure S3. Absolute concentration of non-modified ubiquitin peptides that served as proxy for total ubiquitin during Ub-AQUA-PRM analysis. (a) The unmodified TITLEVEPSDTIENVK peptide and (b) the unmodified ESTLHLVLR peptide. Error bars indicate standard deviation.

Supplementary Figure S4. Atypical polyubiquitin chain types are enriched in certain murine tissues. Differences in total ubiquitin levels were detected between murine tissues and the contribution of atypical linkage types to the total ubiquitin pool was determined. Percentage contribution of (a) K33 and (b) K29 to total ubiquitin in different murine tissues. Error bars indicate standard deviation.

Supplementary Figure S5. Murine tissues contain a large amount of unconjugated ubiquitin. Western blot for total ubiquitin (conjugated and unconjugated) in murine tissues. The same tissues were used as those analysed by Ub-AQUA-PRM.

Supplementary Figure S6. Mitochondrial proteins are enriched in K29/K33 TUBE pulldowns from murine muscles. (a) Gene Ontology overrepresentation analysis of cellular components for proteins identified as enriched in TRABID pulldowns, which recognises K29/K33 ubiquitin chain types. (b) Reactome pathway enrichment of proteins identified as enriched in TRABID pulldowns.

Supplementary Table S1. Peptides used for absolute quantification of ubiquitin chain types by Ub-AQUA-PRM analysis.

Supplementary Table S2. Multi-step gradient used for separating ubiquitin peptides during Ub-AQUA-PRM analysis.

Supplementary Table S3. Proteins identified in TRABID pulldowns from mouse muscle.

Supplementary Table S4. Proteins identified as differentially enriched in TRABID pulldowns from mouse muscle.

Graphical abstract

Highlights:

- Absolute quantification of ubiquitin chain types in 10 minutes
- There are tissue-specific differences in ubiquitin levels in murine tissues
- Atypical ubiquitin chain types are enriched in contractile tissues

Table 1. Proteins enriched in TRABID pulldowns from mouse muscle.

Uniprot ID	Protein name	Unique peptides	log_2 Fold change	*p*-value
Q69ZQ1	Myogenesis-regulating glycosidase	7	2.1	0.000588
P97300	Neuroplastin	2	1.1	0.000952
Q9JK92	Heat shock protein beta-8	5	1.4	0.002102
P67778	Prohibitin	5	1.3	0.002871
Q6P8X1	Sorting nexin-6, N-terminally processed	9	4.8	0.004456
Q60597	2-oxoglutarate dehydrogenase, mitochondrial	34	1.0	0.004607
P0CG49	Polyubiquitin-B	7	2.0	0.006479
P28271	Cytoplasmic aconitate hydratase	11	2.1	0.007295
A2AMM0	Caveolae-associated protein	5	1.1	0.007315
Q9JLT4	Thioredoxin reductase 2, mitochondrial	5	1.5	0.008499
O55023	Inositol monophosphatase 1	11	1.7	0.009204
P58252	Elongation factor 2	42	1.4	0.009641

Supplementary Table S1. Peptides used for absolute quantification of ubiquitin chain types by Ub-AQUA-PRM analysis.

Sequence	m/z	Z	RT (min)	NCE (%)	Transitions
GGM(ox^{2})QIFVK[$^{13}C_6{}^{15}N_2$]	460.2435	2+	6.7	20	y3^{+}, y5^{+}, y6^{+}, y4^{+}, y2^{+}
GGM(ox^{2})QIFVK	456.2364	2+	6.7	20	y3^{+}, y5^{+}, y6^{+}, y4^{+}, y2^{+}
M(ox^{2})QIFVK(**GG**)TLTGK[$^{13}C_6{}^{15}N_2$]	710.3914	2+	7.2	24	y8^{+}, y6^{+}, y9^{+}, y7^{+}, y5^{+}
M(ox^{2})QIFVK(**GG**)TLTGK	706.3843	2+	7.2	24	y8^{+}, y9^{+}, y6^{+}, y7^{+}, y5^{+}
TLTGK(**GG**)TITLEVEPSDTIENVK[$^{13}C_6{}^{15}N_2$]	804.0983	3+	9.3	20	y9^{+}, y9^{2+}, y10^{+}, y19^{2+}, y11^{+}
TLTGK(**GG**)TITLEVEPSDTIENVK	801.4269	3+	9.3	20	y9^{+}, y9^{2+}, y10^{+}, y19^{2+}, y11^{+}
TITLEVEPSDTIENVK(**GG**)AK[$^{13}C_6{}^{15}N_2$]	1055.061	2+	9	22	y11^{+}, y12^{+}, y13^{+}, y3^{+}, y14^{+}
TITLEVEPSDTIENVK(**GG**)AK	1051.054	2+	9	22	y11^{+}, y12^{+}, y13^{+}, y3^{+}, y14^{+}
AK(**GG**)IQDK[$^{13}C_6{}^{15}N_2$]	412.7394	2+	5.7	26	y4^{+}, y2^{+}, y3^{+}, y5^{+}, y5^{2+}
AK(**GG**)IQDK	408.7323	2+	5.7	26	y4^{+}, y2^{+}, y3^{+}, y5^{+}, y5^{2+}
IQDK(**GG**)EGIPP[$^{13}C_5{}^{15}N$]DQQR[$^{13}C_6{}^{15}N_4$]	551.9536	3+	6.3	22	y6^{2+}, y6^{+}, y5^{+}, y5^{2+}, y3^{+}
IQDK(**GG**)EGIPPDQQR	546.6129	3+	6.3	22	y6^{2+}, y6^{+}, y5^{+}, y5^{2+}, y3^{+}
LIFAGK(**GG**)QLEDGR[$^{13}C_6{}^{15}N_4$]	735.9006	2+	7.3	24	y8^{+}, y10^{+}, y10^{2+}, y9^{+}, y2^{+}
LIFAGK(**GG**)QLEDGR	730.8964	2+	7.3	24	y8^{+}, y10^{+}, y10^{2+}, y9^{+}, y2^{+}

TLSDYNIQK(**GG**)ESTLHLVLR[$^{13}C_6{}^{15}N_4$]	752.0737	3+	9.2	20	$y16^{2+}$, $y13^{2+}$, $y15^{2+}$, $y14^{2+}$, $y11^{2+}$
TLSDYNIQK(**GG**)ESTLHLVLR	748.7376	3+	9.2	20	$y16^{2+}$, $y13^{2+}$, $y15^{2+}$, $y14^{2+}$, $y11^{2+}$
ESTESTLHLVLR[$^{13}C_6{}^{15}N_4$]	539.3182	2+	7.2	28	$y5^{+}$, $y4^{+}$, $y3^{+}$, $y5^{2+}$, $y6^{+}$
ESTESTLHLVLR	534.314	2+	7.2	28	$y5^{+}$, $y4^{+}$, $y3^{+}$, $y5^{2+}$, $y6^{+}$
TITTITLEVEPSDTIENVK[$^{13}C_6{}^{15}N_2$]	898.4744	2+	9.5	20	$y9^{+}$, $y10^{+}$, $y11^{+}$, $y12^{+}$, $y14^{+}$
TITTITLEVEPSDTIENVK	894.4673	2+	9.5	20	$y9^{+}$, $y10^{+}$, $y11^{+}$, $y12^{+}$, $y14^{+}$

*Ox^2 = sulfone version of methionine

Supplementary Table S2. Multi-step gradient used for separating ubiquitin peptides during Ub-AQUA-PRM analysis.

Time (min)	**%B**
0	0
4	0
4.25	7
5	12
6	15
7	16
8	24
8.25	35
8.5	90
8.75	90
9	0
10	0

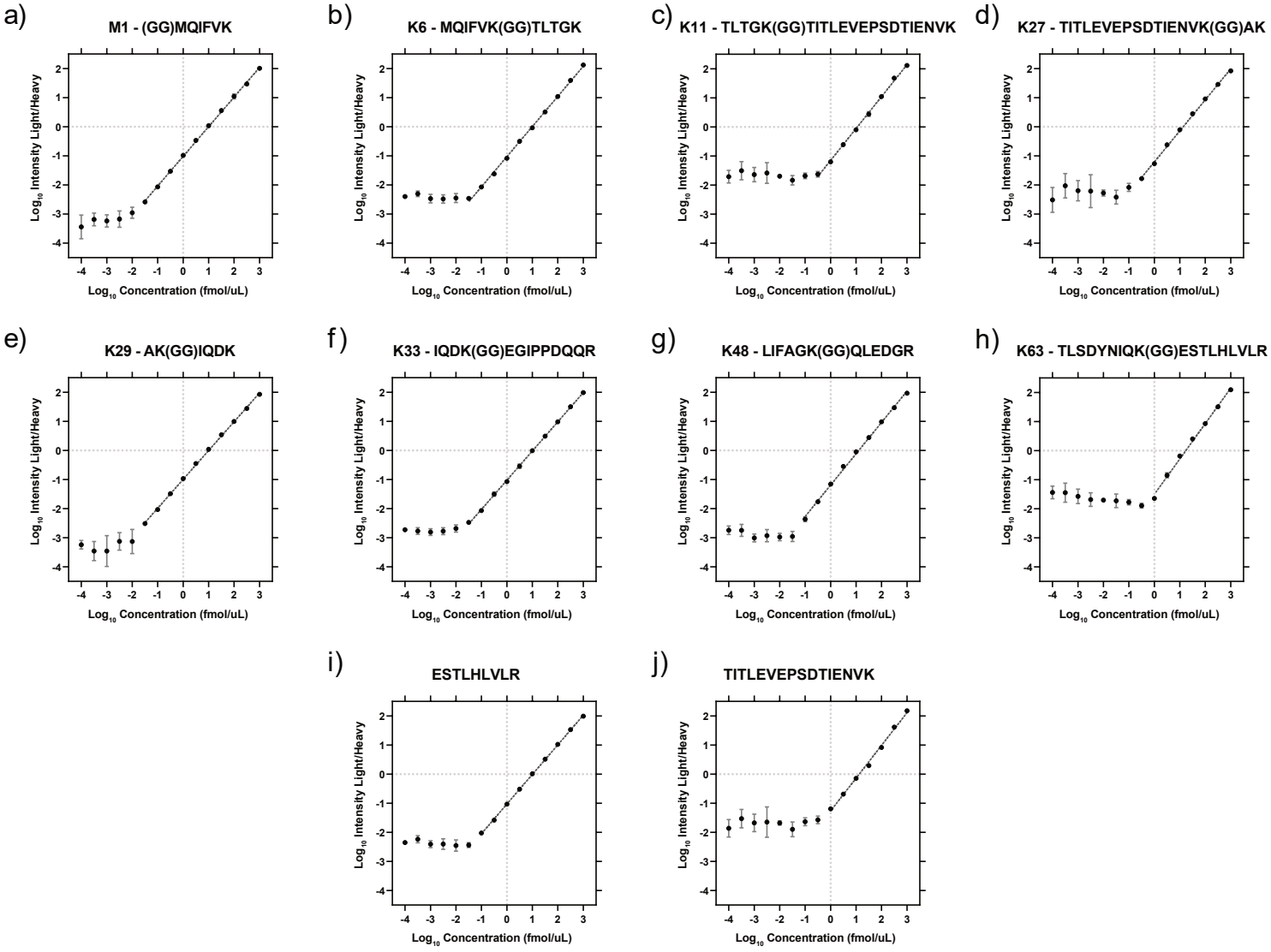
a)
M1 - (GG)MQIFVK
b)
K6 - MQIFVK(GG)TLTGK
c)
K11 - TLTGK(GG)TITLEVEPSDTIENVK
d)
K27 - TITLEVEPSDTIENVK(GG)AK
e)
K29 - AK(GG)IQDK
f)
K33 - IQDK(GG)EGIPPDQQR
g)
K48 - LIFAGK(GG)QLEDGR
h)
K63 - TLSDYNIQK(GG)ESTLHLVLR
i)
ESTLHLVLR
j)
TITLEVEPSDTIENVK
Log10 Intensity Light/Heavy
Log10 Concentration (fmol/uL)

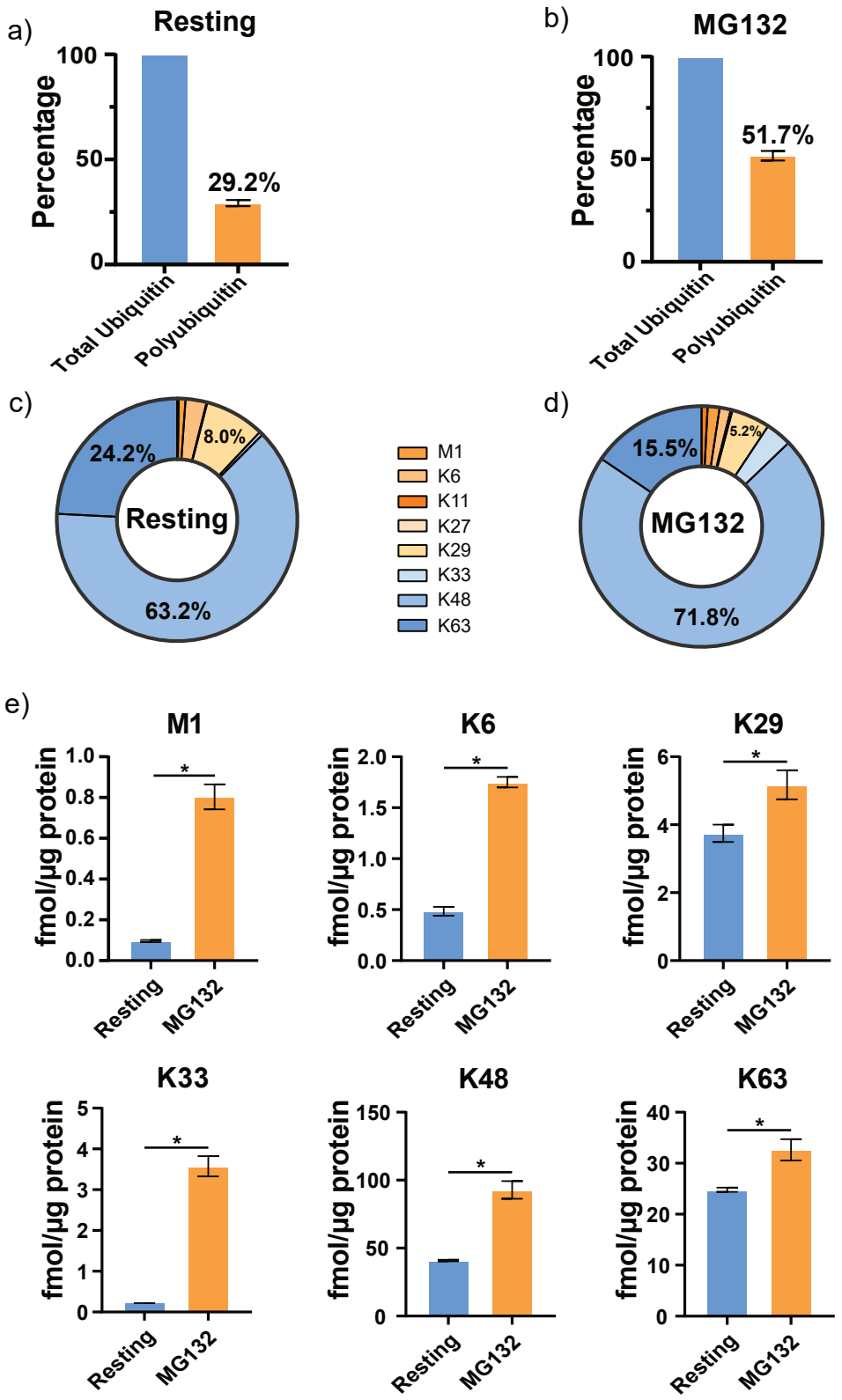
a)
Resting
Percentage
100
50
0
29.2%
Total Ubiquitin
Polyubiquitin
b)
MG132
Percentage
100
50
0
51.7%
Total Ubiquitin
Polyubiquitin
c)
24.2%
8.0%
Resting
63.2%
M1
K6
K11
K27
K29
K33
K48
K63
d)
15.5%
5.2%
MG132
71.8%
e)
M1
K6
K29
K33
K48
K63
fmol/µg protein
Resting
MG132
*

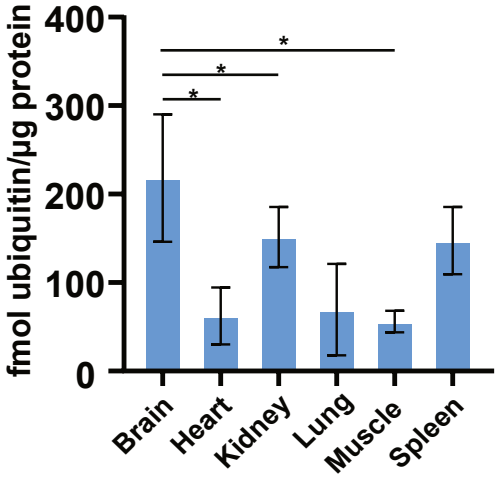
fmol ubiquitin/µg protein
400
300
200
100
0
*
*
*
Brain
Heart
Kidney
Lung
Muscle
Spleen

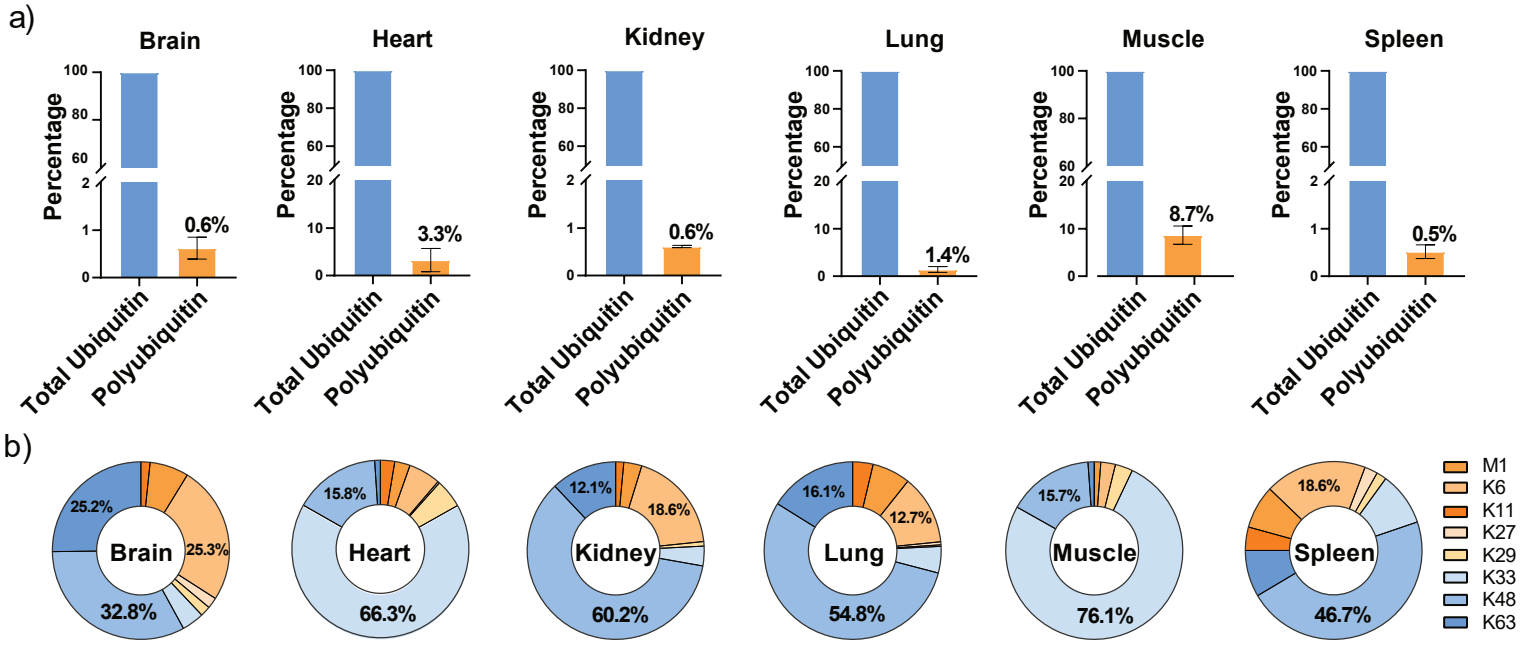
a)
Brain
Heart
Kidney
Lung
Muscle
Spleen
Percentage
0.6%
3.3%
0.6%
1.4%
8.7%
0.5%
Total Ubiquitin
Polyubiquitin
b)
Brain
25.2%
25.3%
32.8%
Heart
15.8%
66.3%
Kidney
12.1%
18.6%
60.2%
Lung
16.1%
12.7%
54.8%
Muscle
15.7%
76.1%
Spleen
18.6%
46.7%
M1
K6
K11
K27
K29
K33
K48
K63

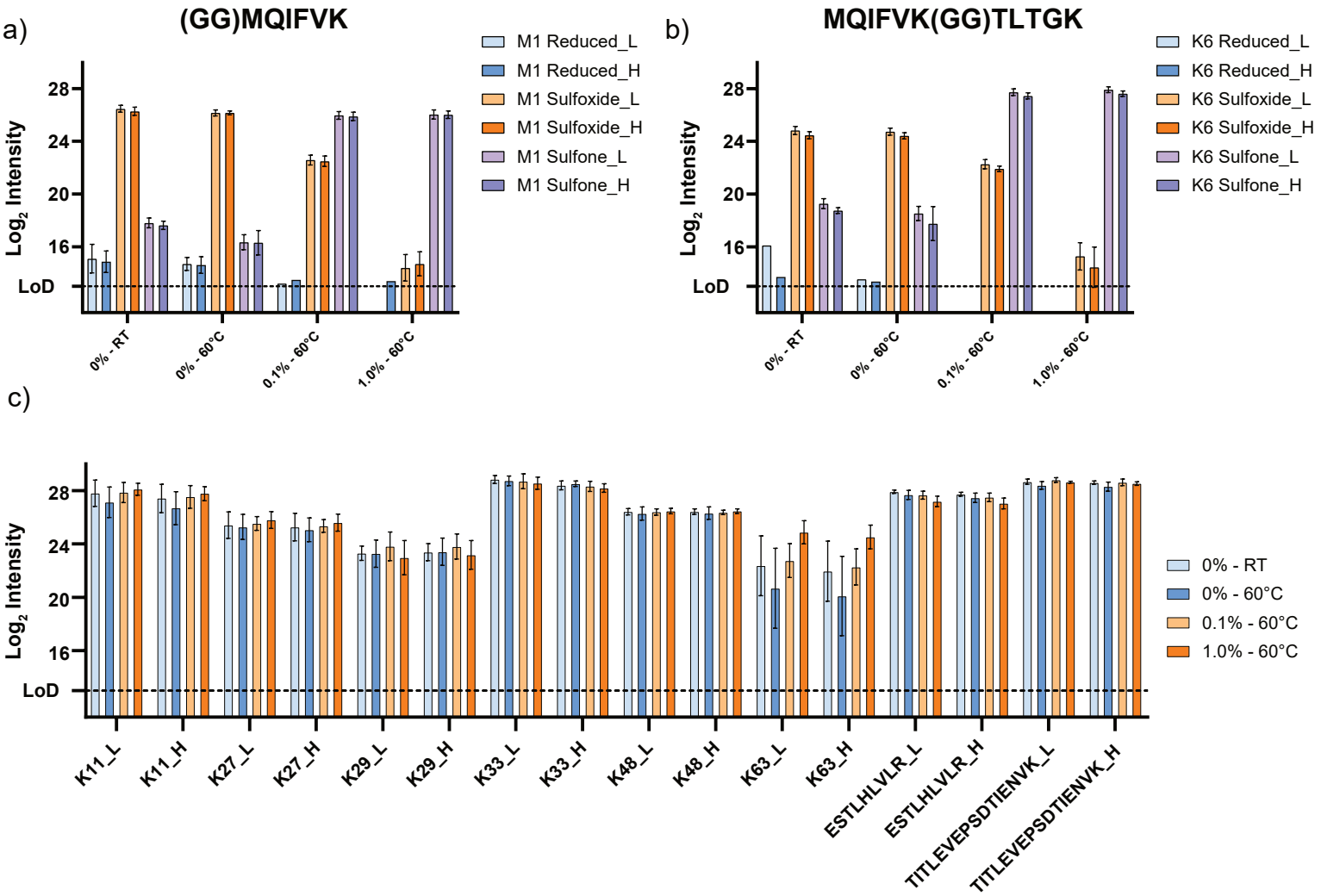
a)
(GG)MQIFVK
M1 Reduced_L
M1 Reduced_H
M1 Sulfoxide_L
M1 Sulfoxide_H
M1 Sulfone_L
M1 Sulfone_H
Log2 Intensity
28
24
20
16
LoD
0% - RT
0% - 60°C
0.1% - 60°C
1.0% - 60°C
b)
MQIFVK(GG)TLTGK
K6 Reduced_L
K6 Reduced_H
K6 Sulfoxide_L
K6 Sulfoxide_H
K6 Sulfone_L
K6 Sulfone_H
Log2 Intensity
28
24
20
16
LoD
0% - RT
0% - 60°C
0.1% - 60°C
1.0% - 60°C
c)
Log2 Intensity
28
24
20
16
LoD
0% - RT
0% - 60°C
0.1% - 60°C
1.0% - 60°C
K11_L
K11_H
K27_L
K27_H
K29_L
K29_H
K33_L
K33_H
K48_L
K48_H
K63_L
K63_H
ESTLHLVLR_L
ESTLHLVLR_H
TITLEVEPSDTIENVK_L
TITLEVEPSDTIENVK_H

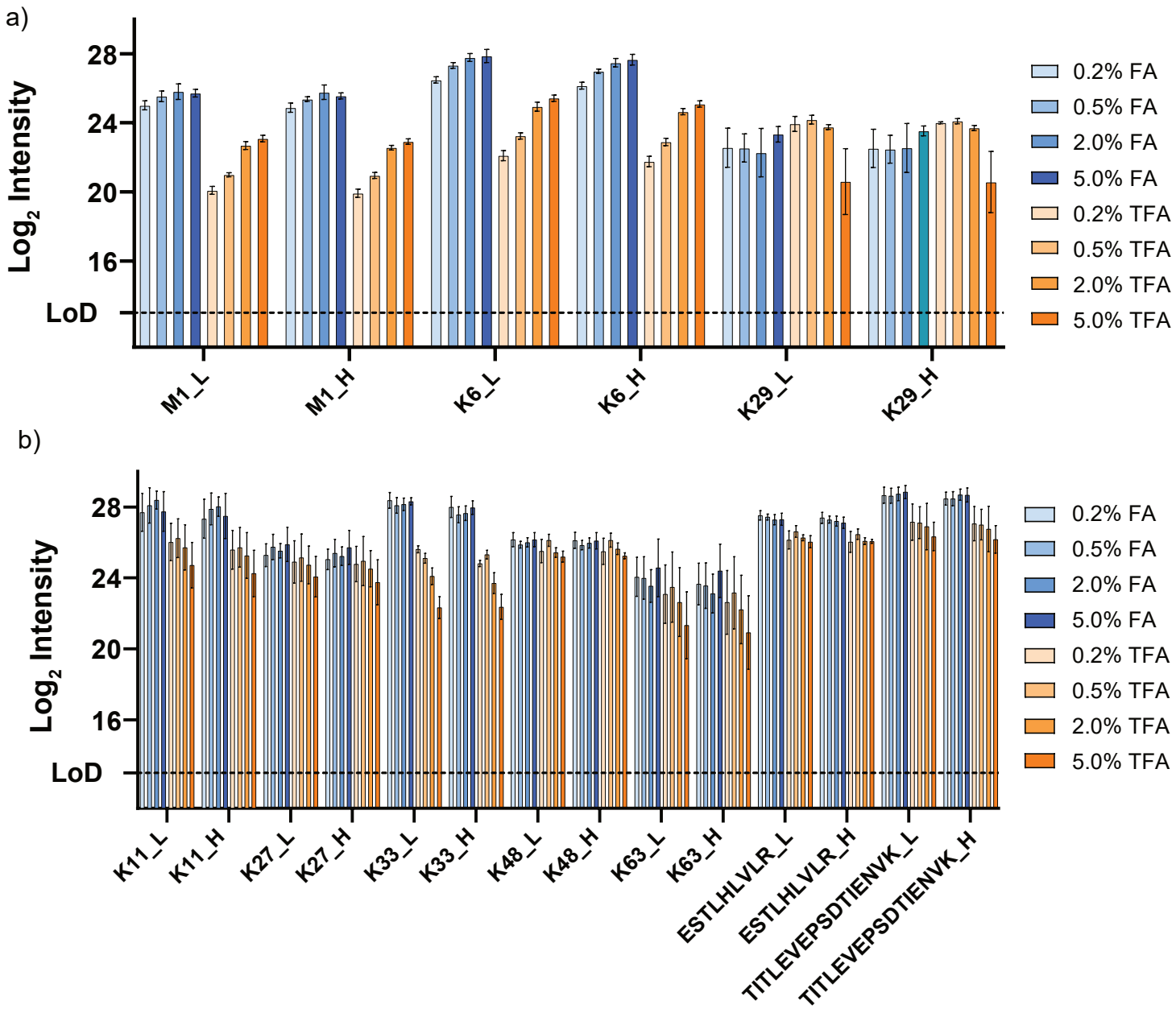
a)
Log2 Intensity
28
24
20
16
LoD
M1_L
M1_H
K6_L
K6_H
K29_L
K29_H
0.2% FA
0.5% FA
2.0% FA
5.0% FA
0.2% TFA
0.5% TFA
2.0% TFA
5.0% TFA
b)
Log2 Intensity
28
24
20
16
LoD
K11_L
K11_H
K27_L
K27_H
K33_L
K33_H
K48_L
K48_H
K63_L
K63_H
ESTLHLVLR_L
ESTLHLVLR_H
TITLEVEPSDTIENVK_L
TITLEVEPSDTIENVK_H
0.2% FA
0.5% FA
2.0% FA
5.0% FA
0.2% TFA
0.5% TFA
2.0% TFA
5.0% TFA

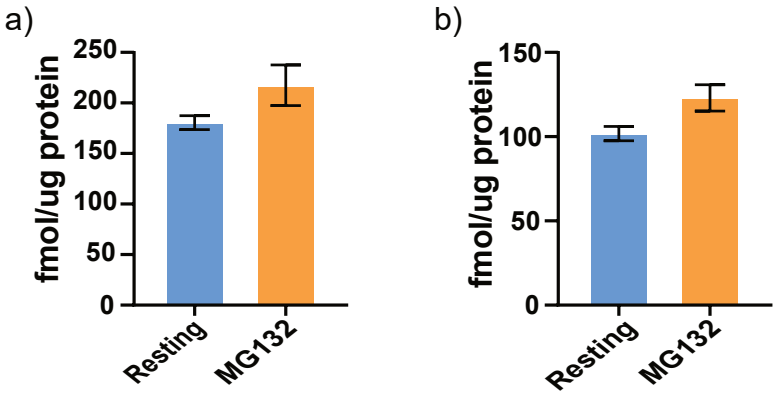
a)
fmol/ug protein
250
200
150
100
50
0
Resting
MG132
b)
fmol/ug protein
150
100
50
0
Resting
MG132

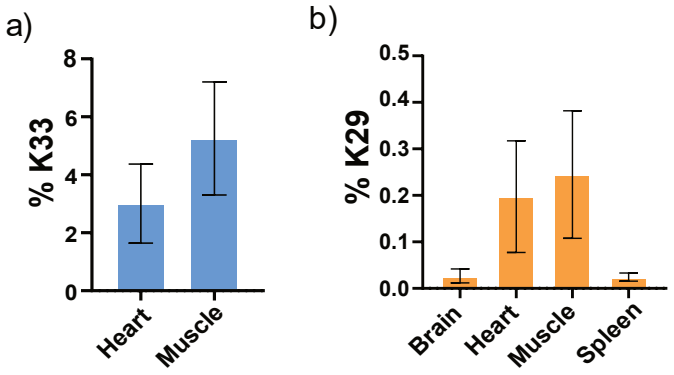
a)
% K33
8
6
4
2
0
Heart
Muscle
b)
% K29
0.5
0.4
0.3
0.2
0.1
0.0
Brain
Heart
Muscle
Spleen

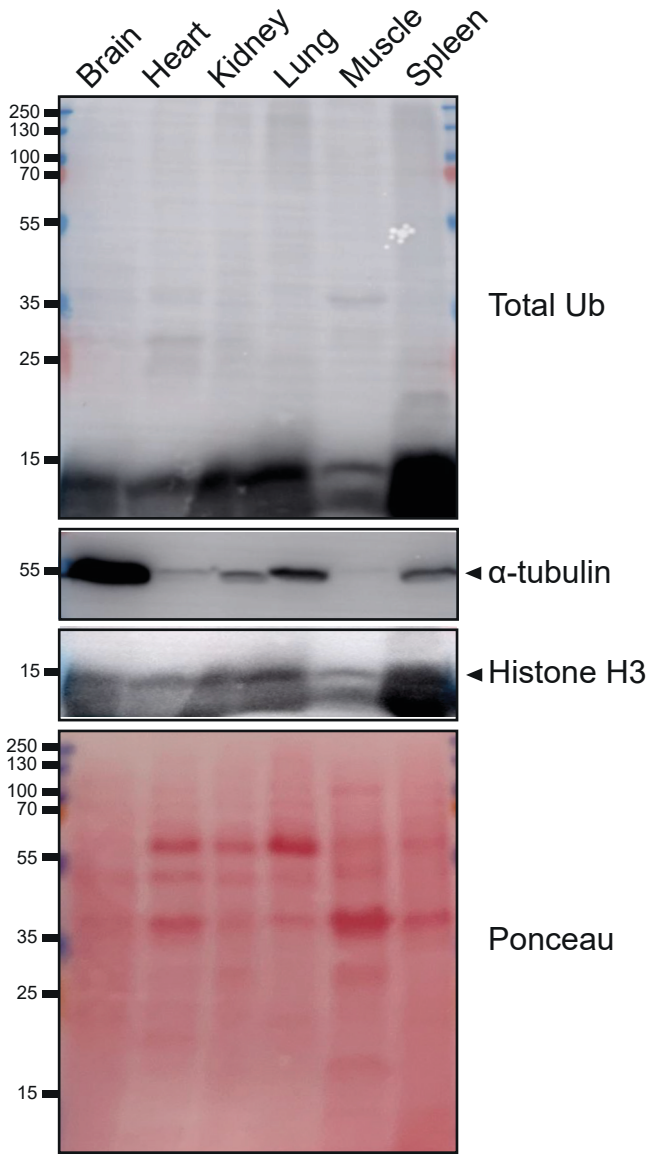
Brain
Heart
Kidney
Lung
Muscle
Spleen
250
130
100
70
55
35
25
15
Total Ub
55
α-tubulin
15
Histone H3
250
130
100
70
55
35
25
15
Ponceau

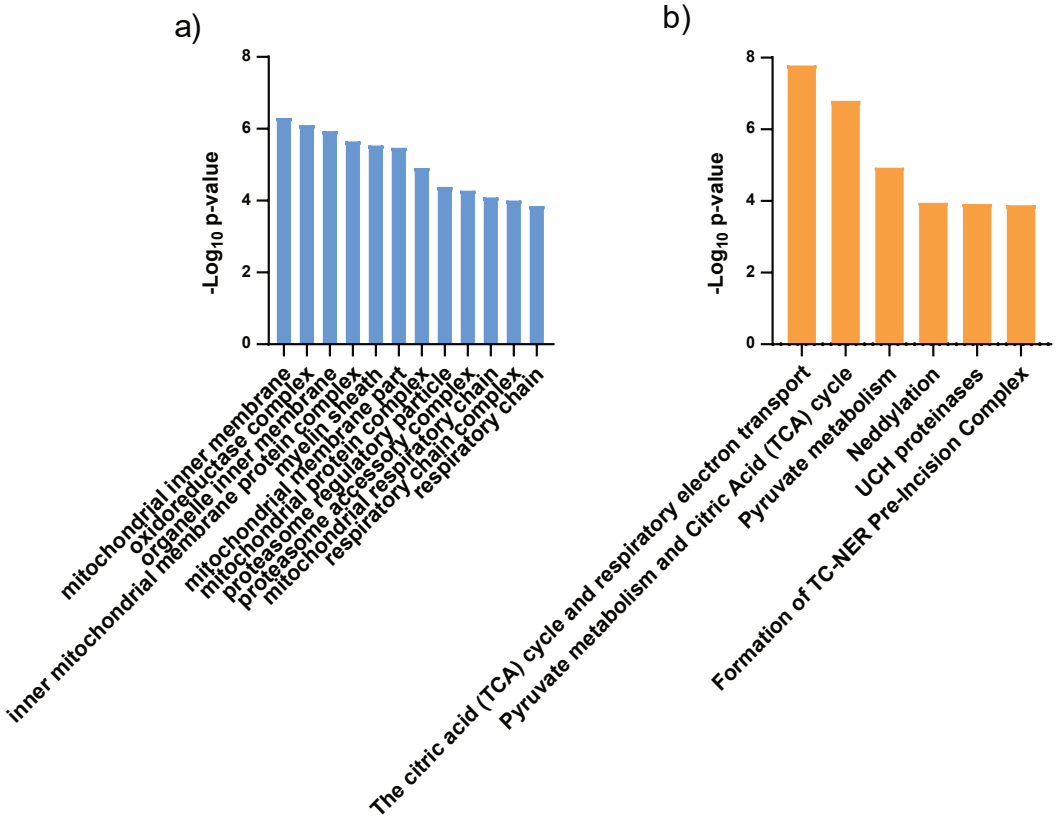
a)
-Log10 p-value
8
6
4
2
0
mitochondrial inner membrane
oxidoreductase complex
organelle inner membrane
inner mitochondrial membrane protein complex
myelin sheath
mitochondrial membrane part
mitochondrial protein complex
proteasome regulatory particle
proteasome accessory complex
mitochondrial respiratory chain complex
respiratory chain
b)
-Log10 p-value
8
6
4
2
0
The citric acid (TCA) cycle and respiratory electron transport
Pyruvate metabolism and Citric Acid (TCA) cycle
Pyruvate metabolism
Neddylation
UCH proteinases
Formation of TC-NER Pre-Incision Complex